CrystEngComm

Stereo-electronic effect of perfluoropropyl group on solid state molecular packing of isomeric dibenzo [a,c]phenazine derivatives

Journal:	*CrystEngComm*
Manuscript ID	CE-ART-01-2022-000019.R1
Article Type:	Paper
Date Submitted by the Author:	25-Jan-2022
Complete List of Authors:	Putta, Anjaneyulu; University of South Dakota, Chemistry Gairhe, Shankar; University of South Dakota, Chemistry Yao, Feng; University of South Dakota, Chemistry Sun, Haoran; University of South Dakota, Chemistry

Stereo-electronic effect of perfluoropropyl group on solid state molecular packing of isomeric dibenzo [a,c]phenazine derivatives

Received 00th January 20xx,
Accepted 00th January 20xx

DOI: 10.1039/x0xx00000x

Anjaneyulu Putta,[a] Shankar Gairhe[a], Yao Feng[a], and Haoran Sun [a*]

We report here the synthesis, characterization, and crystal structures of three perfluoropropylated dibenzo [a,c]phenazine constitutional isomers where the only differences among them are the position of perfluoropropyl substituents. The crystal structures of these perfluropropylated dibenzo [a,c]phenazine isomers indicate that stereo-electronic effect of perfluoropropyl group on dibenzo [a,c]phenazine molecule plays a crucial role in determining the crystal packing motif in the solid state. Our results from both x-ray crystallography and computational approaches reveal that position of the perfluoropropyl groups on dibenzo [a,c]phenazine ring significantly affects the electrostatic potential distribution along the aromatic ring surface, resulting drastic changes in molecular packing in the solid state, from herringbone to lamellar crystal packing among these three constitutional isomers. Simple topological consideration of the molecular packing in the solid state is coincidently cooperative with the changes in electrostatic potential distributions where localized partial positive and partial negative charges, perhaps dominate the intermolecular interactions between aromatic rings. Together, the perfluoropropylation on the dibenzo [a,c]phenazine ring provides us a fortunate scenario where molecular topological structure and electrostatic potential works together to facilitate the formation of desired lamellar π-π stacked crystal packing. The meantime, elctrochemistry, UV-visible absorption and emision spectra, and computational chemistry results point out that there are only minor to moderate changes of electronic properties of the molecules upon changing the position of the perlfuoroalkyation on the dibenzo [a,c]phenazine core. While controlling the solid state structure of aromatics by design is still a long way to go, we hope that our work could ignite a spark that can potentially spread into the field of design of organic solid state materials.

1 Introduction

Despite the recent advancement of organic semiconductor materials,[1, 2] design of new, small molecular organic semiconductor materials with predictable crystal packing motif and electronic properties is yet still a significant challenge,[3, 4] due to the coexisting weak intermolecular interaction forces which are often various a few kcal/mol the most.[5, 6] Modification of the molecular structure of organic semiconductors, i.e. changes in the size of π conjugation,[7, 8] changes in substitutions of the π conjugation,[9-11] and doping of hetero atoms into the π conjugation,[12-14] generally provides predictable electronic properties changes at the molecular scale. However, such modification at the molecular level often results in unpredictable electronic properties for the bulk materials where such properties are governed by structure at both molecular and bulk solid state levels.[15, 16] For example, molecules with same size/shape π system but different substituents can have drastic difference in their electronic properties due to the difference in molecular packing motifs in the solid state.[17, 18]

Crystal packing mode in organic semiconductor materials can be altered through several strategies, though still at the trial-and-error stage.[19-21] Generally, molecules with ionic and/or coordination binding ability often show better capability in forming a desired solid state packing in a controllable fashion.[22, 23] However, the introduction of charged species and/or metal ions will likely significantly alter the electronic properties of the original π system used in such materials though it shows significant benefits in other applications such as catalysis and energy storage.[24, 25] Another widely used approach is to utilizing strong hydrogen bonding network to build a desired solid state molecular packing motif, providing many successful cases in controlling semiconductor properties.[26-28]

In the meantime, many promising organic semiconductor molecules lack the ability to form such hydrogen bonding network or possess significant challenge to do so.[29-31] The solid state structures of these types of organic semiconductors are controlled by intermolecular non-covalent bonding including dipole-dipole, quadrupole-quadrupole, dipole-quadrupole, dipole, and induced-dipole interactions.[32, 33] While these weak non-covalent bonding interactions are typically electrostatic in nature, prioritizing one type over others among these non-covalent intermolecular interactions is key toward controlling solid state structures in bulk, resulting in controlled electronic properties of the bulk organic semiconductor materials.[34-36]

Introducing electron-withdrawing groups onto aromatics is one of the strategies to control the crystal packing of organic semiconductor materials in the solid state.[37-40] Perfluoroalkyl group is one of the most versatile electron-withdrawing groups often added onto aromatic cores to improve air-[41-44] and photo-stability of aromatic molecules.[45-48] Molecular orbitals and their energy levels are also modulated by adding perfluoroalkyl groups to aromatic molecule.[49, 50] Over the past, we have identified that localization of partial charges along the π system surface, represented by difference on the molecular electrostatic potential (ESP) maps, plays a key role in controlling the molecular packing among the dibenzo [a,c]phenazine

[a] Department of Chemistry and Center for Fluorinated Functional Materials, University of South Dakota, Vermillion, South Dakota, United States, 57069. Email: Haoran.Sun@usd.edu

† Footnotes relating to the title and/or authors should appear here.
Electronic Supplementary Information (ESI) available: [synthetic procedures and characterization data of compounds 1 and 3, crystal structure analysis results, computational chemistry procedures and coordinates of optimized geometries and total energies of compounds 1, 2, and 3]. See DOI: 10.1039/x0xx00000x

derivatives.[51] Among the perfluoroalkyl substitutions (typically n-perfluorobutyl substituent) on the aromatic ring, we were able to achieve lamellar π-π stacked molecular packing motif with less than 3.4 Å interplanar distance in the solid state.

In addition to the strategies used in our previous work,[52, 53] including the introduction of perfluoroalkyl substituents, increasing the size of π conjugation, and introduction of highly polarizable soft hetero atoms into the π system, we thought to purposely introduce perfluoroalkyl substituents onto different positions of the π system to create isomers that possess the same substituents and the π system. The only difference between these constitutional isomers is the position of the substitution. This approach provides us an opportunity to probe how the substitution position can affect the electronic properties of the large π system, an analog question to the benchmark benzene derivatives, ortho and para vs meta effects. More importantly, how it would further extend its stereo-electronic properties to influence the molecular packing in crystal structures.

Here, we chose a medium size dibenzo [a,c]phenazine ring as the π system for our study due to its electron accepting capability and planar structure.[54] Moreover, dibenzo [a,c]phenazine is used as a promising n-type building block in the research and development of organic semiconductor materials ranging from OLEDs, solar cells, catalysts, and phototransistors.[55-58] Despite their potential applications in organic semiconductor field, the crystal structure and analysis of crystal packing of dibenzo [a,c]phenazine derivatives were reported scarcely.[59, 60]

Built on the foundation of our earlier work on perfluoroalkylated polyaromatic hydrocarbons (PAHs),[51-53, 61] we report here the synthesis, characterization, and crystal structures of three isomers of perfluoropropylated dibenzo [a,c]phenazine. Together with DFT calculation results, we further discuss the stereo-electronic effects of the perfluoroalkyl group on both crystal packing and electronic properties of these three isomers.

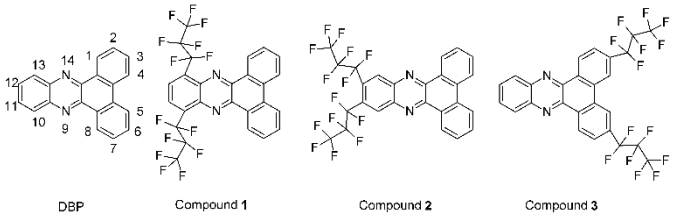

Chart 1: Molecular structures of compounds in this study. Dibenzo [a,c]phenazine (DBP) with ring numbering and compounds **1**-**3**. DBP is a commercial compound and compound **2** reported in our previous work.

2 Results & Discussion

2.1 Synthesis:

For compound **1** synthesis, first 10,13-dibromo dibenzo [a,c]phenazine (PBrDBP) was synthesized from the condensation of 3,6-dibromo-1,2-phenylene diamine with 9,10-pheanthrenequninone. Then, compound **1** was synthesized from 10,13-dibromo dibenzo [a,c]phenazine via copper-mediated cross-coupling reaction using perfluoropropyl iodide and Cu powder in 54% yield as shown in Scheme **1.** Compound **2** was prepared by reacting n-perfluoropropyl iodide with 11,12-dibromo dibenzo [a,c]phenazine in presence of Cu powder in a mixture of solvents DMSO and HFE-7200 with 13% yield. The intermediate 11,12-dibromo dibenzo [a,c]phenazine was prepared by condensation of 4,5-dibromo-1,2-phenylene diamine with 9,10-phenanthrene quinone. The synthetic method used for compound **3** was not attempted for preparation of compound **2** as the synthesis of 4,5-bisperfluoropropyl-1,2-phenylene diamine involves multiple synthetic steps and challenges to be synthetically successful. Compound **3** was synthesized using a modified procedure from our previously reported method. First, the key intermediate 3,6-bisperfluoropropylphenanthrene-9,10-dione was synthesized from 3,6-dibromophenanthrene-9,10-di(ethylene glycol)ketal followed by perfluoropropylation and deprotection of the ketal. Condensation reaction between 3,6-bisperfluoropropylphenanthrene-9,10-dione and 1,2-phenylene diamine gave compound **3** in 95% yield.

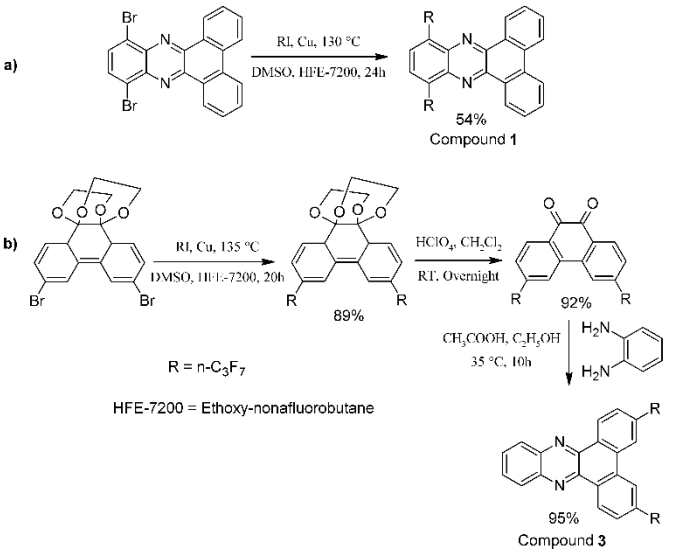

Scheme 1: Reaction schemes for the synthesis of compound **1**(a), compound **3**(b).

2.2 Effect of n-perfluoropropyl groups position on crystal packing: Crystal structure analysis

Single crystals of compound **1** were obtained by slow evaporation of saturated dichloromethane solution for several days. Single crystals of compound **3** suitable for x-ray diffraction were obtained by layered liquid-liquid diffusion method. First, concentrated solution of compound **3** in dichloromethane was prepared and methanol was added carefully on top of the dichloromethane solution along the side wall of the small vial The small vial was sealed and put in a quiescent place to avoid strong vibration for several days to yield light-yellow needle crystals. Compound **1** crystallized in monoclinic system with

space group P 21/c, while compound **3** crystallized in monoclinic system with space group C2/c.

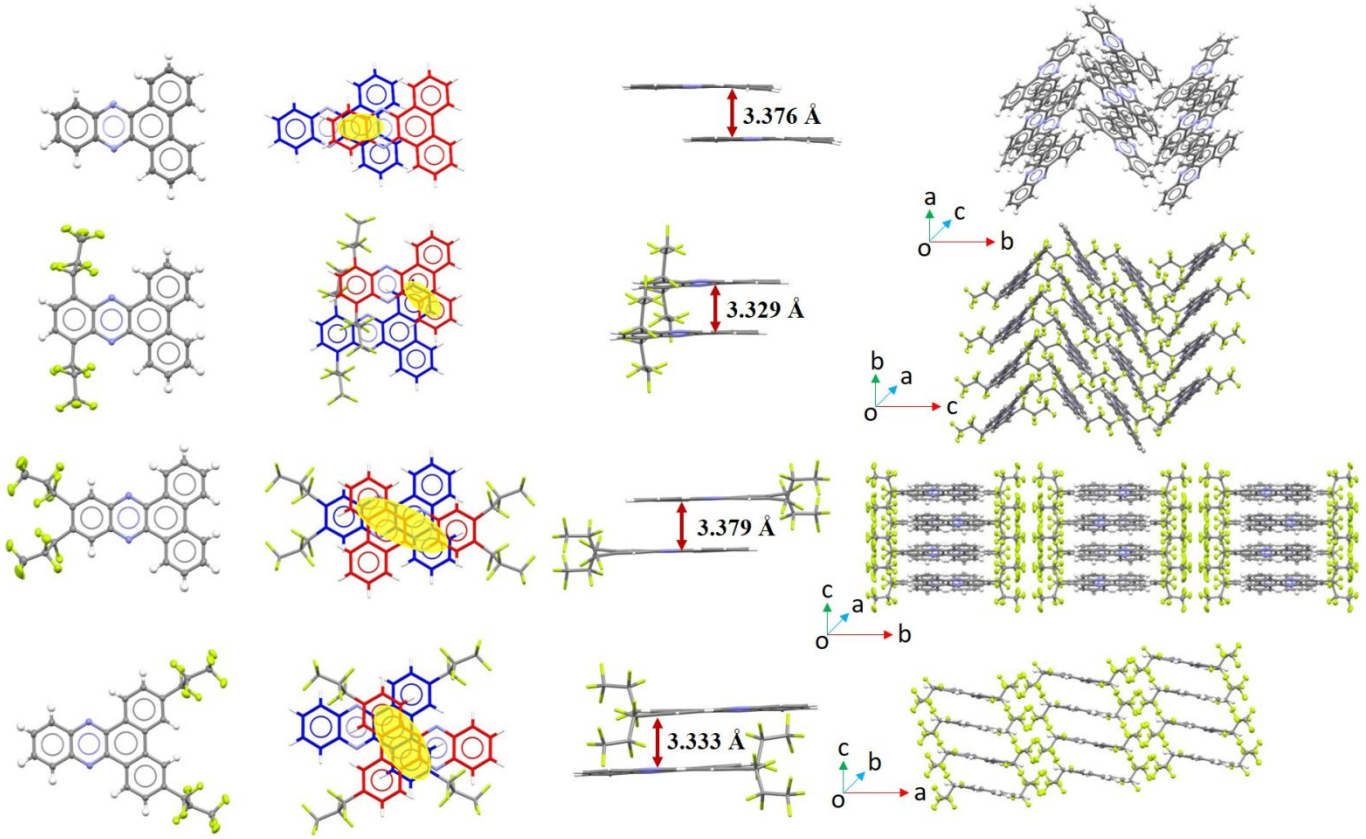

Figure 1: Crystal structure, top view of dimer with π overlapping (yellow oval), interplanar distance in dimers and crystal packing (left to right) of DBP, compounds **1**, **2,** and **3** (from top to bottom). The interplanar distance was calculated between two adjacent dibenzo [a,c]phenazine molecules with the plane was defined by the average of the 22 non-hydrogen atoms of the dibenzo [a,c]phenazine ring.

Analysis of single crystal structures, crystal packing mode and non-covalent interactions is of great importance to understand the electronic properties of the organic materials. The crystal packing of unsubstituted dibenzo [a,c]phenazine (DBP) showed herringbone pattern with minimal π-π overlaping between aromatic rings. Upon adding n-perfluoropropyl group on the parent dibenzo [a,c]phenazine aromatic ring at 10,13-positions(compound **1**), the crystal packing showed herringbone pattern similar to the pattern showed in unsubstituted dibenzo [a,c]phenazine (DBP). While upon changing the substitution position of n-perfluoropropyl group on dibenzo [a,c]phenazine from 10,13-position to 11,12-position (compound **2**), the crystal packing has changed to lamellar, though with some imperfection. When the n-perfluoropropyl groups added onto 3,6-positions (compound **3**), the crystal packing dramatically changed from herringbone to perfect lamellar pattern. This change in crystal packing is due to the decrease of intermolecular interactions in C···H, F···C and the increase of C···C in the case of compound **3** which lead to lamellar packing. Substitution at 10,13-position (compound **1**) resulted in slipped face-face stacking with overall herringbone packing. While substitution of n-perfluoropropyl groups at 11,12-position (compound **2**)[51] and 3,6-position (compound **3**) resulted in anti-parallel mode with overall lamellar packing. π overlapping area decreased in the case of compound **1** compared to compound **2** and **3**. Due to the slipped parallel packing, only a portion of aromatic rings overlap in compound **1** which can be seen from **Figure 1**.

Slight changes in the interplanar distance among these three isomers were observed. With the presence of n-perfluoropropyl group at 11,12-position in compound **2**, the π-π distance between two adjacent molecules is 3.379 Å, which is the largest π-π distance among all isomers in this study. By changing the position of n-perfluoropropyl groups to the phenanthrene ring side as in the case of compound **3**, π-π distance was decreased to 3.333 Å. The π-π distance observed in our previous work for n-perfluorobutyl analogue of compound **3** was 3.400 Å.[53] By reducing the chain length from n-perfluorobutyl[53] to n-perfluoropropyl (compound **3**, present work), π-π distance was decreased which is in line with our previous observation, while maintaining the same lamellar packing. Whereas, changing the position of n-perfluoropropyl groups to 10,13-position in the case of compound **1**, shortest π-π stacking distance of 3.329 Å was observed. Although the shortest interplanar distance was observed in the case of compound **1**, slipped parallel packing motif shows the poorest overlapping among these three isomers (**Figure 1**). The network in the crystal packing of compound **1** showed C_{sp2}-H···F-C_{sp3} and

C_{sp2}···F-C_{sp3} intermolecular interactions along the b direction. The crystal of compound **2** forms a 3D network through C_{sp3}-F···F-C_{sp3} intermolecular interactions along the c direction. Compound 3 also forms a 3D network through a combination of C_{sp3}-F···F-C_{sp3} and C_{sp2}-H···F-C_{sp3} intermolecular interactions along the c direction.

Hirshfeld surface analysis was used to investigate different types of intermolecular interactions among all three isomers. From the bar graphs that represent the percentile of different types of intermolecular interactions (**Figure S12**), we can clearly observe that upon changing n-perfluoropropyl substitution position from compound **1** to compound **3**, the contribution of the C···C intermolecular short contacts increases. In the meantime, the amount of the F···C, C···H short contacts decreases. The increase in the C_{sp3}-F···π (F-C) and C_{sp2}-H···π (C-H) interactions favours T-shaped structures leading to overall herringbone packing in compound **1**. For compound **3**, the major dominant short contacts are F···H, F···F, C···H and C···C short contacts. From the 2D fingerprint plots (**ESI**, **Figure S9-S11**), a clear difference in intermolecular interactions was observed upon changing the substitution position of n-perfluoropropyl group from compound **1** to compound **2** and **3**.

2.2 Effect of n-perfluoropropyl groups position on photophysical and electrochemical properties

The UV-Visible absorption and emission spectra of compounds **1**-**3** in dilute dichloromethane solution are shown in **Figure 2**. The absorption maximum (λ_{max}) for compound **1** and **2** found to be 404 and 401 nm respectively, whereas for compound **3** the λ_{max} is 389 nm, which is 15 nm blue shift in the absorption maximum in comparison to compound **1**. Emission maximum for compounds **1** and **2** are 499, 492 nm respectively, whereas for compound 3, blue shift (83 nm) in the emission maximum (416 nm) was observed. The absorption and emission behaviour of these isomers are in good agreement with the calculated band gaps (**Table 1**).

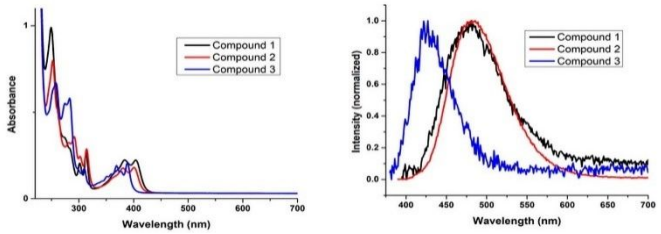

Figure 2: UV-Visible absorption (left) and emission (right) spectra of compounds **1**-**3** in dichloromethane solution.

The fundamental electrochemistry properties of compounds **1**-**3** were measured by cyclic voltammetry in 1,2-difluorobenzene/0.1 M $TBAPF_6$ solution (**Figure 3**). A reversible first redox couple was observed for all these three compounds. One-(compounds **1** and **2**) or two-(compound **3**) irreversible reduction peaks were observed after the first reversible redox couple. The first reversible redox couple represents a single

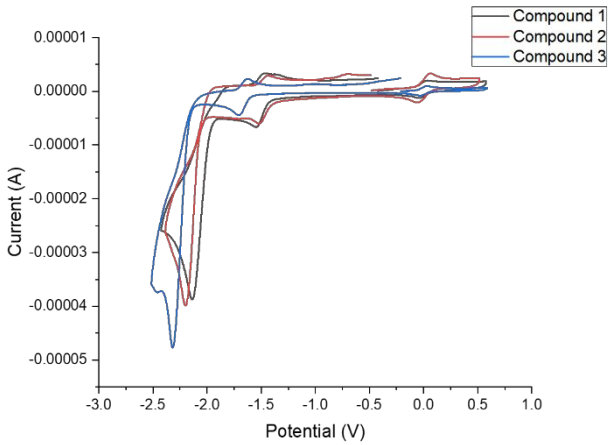

Figure 3: Cyclic voltammogram (CV) of compound **1**(grey), compound **2**(red), compound **3**(blue) at 100 mV/s potential sweep rate in 0.1 M $TBAPF_6$/1,2-difluorobenzene solution. The potential was corrected with Fc/Fc^+ redox couple (shown as the reversible redox couple at 0.0 V in the figure) by adding ferrocene into the solution during the electrochemistry experiments.

electron transfer redox process of the phenazine aromatic ring. Substitutional impact of these compounds is reflected by the difference of redox potentials between compounds **1**, **2**, and **3**. Compounds **1** and **2** show very similar first reduction potentials with less than 50 mV difference between these two, while compound 3 shows its first reduction potential at a much negative potential as shown in **Figure 3**. These results are consistent with our electron affinity (EA) calculation (*vide infra,* **Table 1**) where compounds **1** and **2** have very similar EA values and both values are higher (easier to be reduced) than that of compound **3**.

2.3 Effect of n-perfluoropropyl groups position on electronic properties: Computational approach

Electronic properties of n-perfluoropropyl dibenzo [a,c]phenazine isomers were further studied by Density Functional Theory (DFT) at B3LYP/6-311G(d,p) level of theory in detail. Molecular orbital energy, ionization potential (IP) and electron affinity (EA), reorganization energy (λ) associated with charge transfer were calculated as shown in **Table 1**. Due to the large size of dibenzo [a,c]phenazine aromatic system, for geometry optimization and sequential frequency calculation, we chose trifluoromethyl (CF_3) group to represent n-

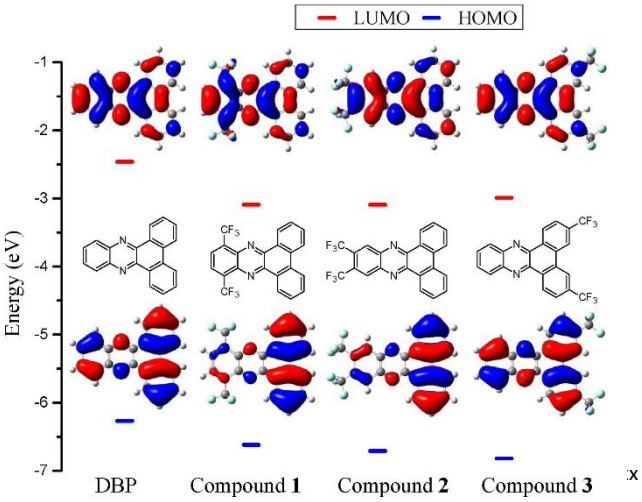

Figure 4: Changes in HOMO, LUMO energy upon changing the substitution position of trifluoromethyl group on dibenzo [a,c]phenazine with comparison to non-substituted dibenzo [a,c]phenazine (DBP).

perfluoropropyl (n-C_3F_7) group which has very similar electronic effect.[62]

The optimized molecular structures of compounds **1**-**3** from DFT calculations were planar and no twisting of the aromatic rings was observed due to trifluoromethyl groups, which has very less steric effect. Whereas, in the case of the crystal structure of compound **1**, moderate twisting was observed due to the reason that one n-perfluoropropyl group faces upward and another n-perfluoropropyl group faces downward and causes steric strain on the aromatic ring. Crystal structures of compound **2** and **3** maintains planar structure.

HOMO for compounds **1** and **2** mainly concentrates on the side of the phenanthrene ring, which indicates the donor character (**Figure 4**). Whereas for compound **3**, the HOMO is located on the overall phenazine ring. The large delocalization of the HOMO provides further stabilization energy, resulting compound **3** possess the lowest HOMO energy among these phenazine isomers. LUMO locates over the central phenazine ring in all three isomers (**Figure 4**). Compound **3** has relatively lower HOMO energy (-6.82 eV) compared to compounds **1**(-6.62 eV) and compound **2**(-6.71 eV). LUMO energy for compound **1** and **2** are the same (-3.09 eV), while LUMO energy for compound **3** is higher (-2.99 eV) compare to compounds **1** and **2** (**Table 1**). HOMO-LUMO energy gap is much higher for compound **3** (3.83 eV) compared to compound **1** (3.53 eV) and compound **2** (3.62eV). These results demonstrate the fine-tuning potential of n-perfluoropropyl substituent on dibenzo [a,c]phenazine molecular orbitals and corresponding energies through isomerization.

Further, we studied the effect of varying substitution positions of trifluoromethyl group on ionization potential, electron affinity and reorganization energy. From **Table 1**, it is clear that compounds **1** and **2** have almost the same electron affinity values (1.83 eV and 1.84 eV), while compound **3** has lower electron affinity value (1.72 eV) indicating that compound **1** and **2** are easier to be reduced compared to compound **3**. The calculated ionization potentials from **Table 1** showed that compound **3** has the highest ionization potential value (8.22 eV) compared to compound **2** (8.18 eV) and compound **1** (8.06 eV) indicating that compound **3** is more difficult to oxidized among all three isomers in this study. From **Table 1**, reorganization energy for electron transfer (ET) for compound **3** is the lowest among all three trifluoromethylated phenazine isomers, and it is very close to DBP (non-substituted phenazine). Reorganization energy of hole transfer for compound **3** (0.222 eV) is close to the corresponding that of electron transfer (0.235 eV). These results suggest that by varying the substitution positions of trifluoromethyl group on dibenzo [a,c]phenazine, the electronic properties could be potentially tuned.

Table 1: Change in electronic properties upon changing the substitution position of trifluoromethyl group on dibenzo [a,c]phenazine by DFT method at B3LYP/6-311G(d,p) level. IP-ionization potential, EA-electron affinity, λ^h_i-reorganization energy for hole transfer, λ^e_i-reorganization energy for electron transfer, DM-dipole moment.

Compounds	E_{HOMO}/eV	E_{LUMO}/eV	E_{Gap}/eV	IP/eV	EA/eV	λ^h_i/eV	λ^e_i/eV	DM/Debye
DBP	-6.27	-2.46	3.81	7.58	1.14	0.280	0.201	0.35
1	-6.62	-3.09	3.53	8.06	1.83	0.210	0.301	2.47
2	-6.71	-3.09	3.62	8.15	1.84	0.220	0.276	6.68
3	-6.82	-2.99	3.83	8.22	1.72	0.222	0.235	5.38

It is not a surprise that a higher dipole moment has been observed for compound **2** (6.68) followed by compound **3** (5.38) and least for compound **1** (2.47) due to the different position of highly electron-withdrawing trifluoromethyl groups on the phenazine ring. Compound **2** and **3**, both trifluoromethyl groups work together with their local dipole cumulate together to amplify the dipole of the entire molecule. Two local dipole moments generated by trifluoromethyl substituents on the opposite position of the phenazine ring in case of compound **1** cancel out, however, their electron-withdrawing effect still changes the electron density of the local phenyl ring they are attached to, making the phenyl ring more electron deficient. This result in a moderate overall dipole moment for compound **1** compared to DBP (non-substituted phenazine).

Change of the n-perfluoropropyl substitution position further alters the electrostatic potential (ESP) distribution among the phenazine surface (**Figure 5**). As shown in **Figure 5**, the ESP maps indicate that perfluoropropylation makes the aromatic ring more electron-deficient in general compared to non-substituted phenazine (**DBP**),[63] while compound **1** having moderate increase in electron deficiency on the ring. Compounds **2** and **3** show greater electron deficiency on the phenazine ring compared to that of compound **1**, while compound **3** is slightly more electron deficient than compound **2**. Further, ESP maps show clearly the steric hindrance of the two n-perfluoropropyl groups when they reside next to each other on two adjacent carbon atoms of the phenyl ring. As expected, two nitrogen atoms within the phenazine ring provide large unevenly distributed electrostatic potential on the

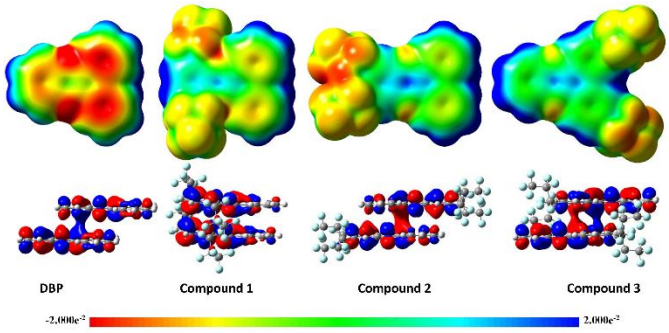

Figure 5: Comparison of electrostatic potential (ESP) maps mapped on total electron density for compounds **1**-**3** and corresponding non-substituted dibenzo[a,c]phenazine (DBP) calculated at M06-2x/TZVP method and basis set. Initial geometries were taken from the crystal structures and calculated the single point energy. The color scale bar at the bottom of the figure is for the relative ESP maps shown in this figure.

phenazine surface, which helps maximize the electrostatic interactions in the dimer molecules.

Together with the "steering effect"[51, 53] of the n-perfluoropropyl groups, this unevenly distributed ESP along the aromatic surface assists to build lamellar π-π stacked crystal packing for compounds **2** and **3**. However, for compound **1**, localized electron-rich regions caused by nitrogen atoms were overlapped with the large n-perfluoropropyl groups, resulting in a block effect for another phenazine ring from overlapping with it to a greater extend.

Dimer interaction energy among the dimers of the compound **1**-**3** were calculated computationally using the crystal structure at M06-2X/TZVP method and basis set with BSSE correction.[64-66] Similar dimerization energies for compound **2** (-17.2 kcal/mol) and compound **3** (-16.4 kcal/mol) were observed. Both of them are much higher than that of compound **1** (-12.8 kcal/mol) which is in line with the ESP maps (**Figure 5**) and crystal packing discussed earlier (**Figure 1**).

Again, compound **3** has relatively similar LUMO overlapping (**Figure 5**) when compared to that of compound **2**. While there is almost no LUMO overlapping for compound **1** due to very small overlapping area in its crystal packing. No HOMO overlapping was observed for the dimers of all three isomers in this study. These results suggest that the presence of n-perfluoropropyl groups on 3,6-positions of dibenzo [a,c]phenazine provide ideal lamellar crystal packing with effective π overlapping and smaller interplanar distance.

3 Conclusions

In summary, we have successfully prepared and characterized three n-perfluoropropyl dibenzo [a,c]phenazine isomers where the only difference is the position of n-perfluoropropyl group substitution. We observed that the crystal packing motifs in these three isomers were changed from herringbone with minimum π system overlapping to perfect lamellar with much better π system overlapping by simply changing the substitution position of n-perfluoropropyl groups on dibenzo [a,c]phenazine ring. Our computational chemistry results showed that changing the n-perfluoropropyl substituent position not only changed the steric hindrance on the perpendicular direction of π system but also drastically changed the electrostatic potential distribution for the corresponding π system. Exemplified with the solid state structure of compound **3**, a cooperative relationship between enhanced electrostatic interaction between π systems and reduced steric hindrance of the perfluoroalkyl substituents on the same π system is likely one of the key factors to the formation of a perfect lamellar packing motif in a perfluoroalklyated polyaromatics. Finally, redox potential, electronic spectra, and DFT calculation results are consistent, together, pointing out that there are only minor to moderate changes of electronic properties of the molecules upon changing the position of the perlfuoroalkyation on the dibenzo [a,c]phenazine ring, while the solid state structures of these constitution isomers are significantly different. With that, we can reasonably predict that one can possibly tune the solid state structure of an organic semiconductor by simply changing the perfluoroalkylation position yet without significantly alternating the electronic properties of the semiconductor core.

4 Experimental Section

General

Chemicals and solvents were purchased from commercial sources and used as received. NMR spectra were collected using $CDCl_3$ as solvent. ^1H and ^{19}F NMR were recorded on a Bruker Avance III HD 400 MHz NMR spectrometer and the chemical shifts were reported in parts per million (ppm). Mass spectra were recorded on GC-2010 plus Shimadzu, Varian 500-MS, Thermo Scientific QExactive Plus orbitrap mass spectrometers with EI and ESI techniques. Elemental analyses were carried out using Exeter Analytic (CE-440) with helium as carrier gas. Crystallographic data were recorded on Bruker D8 Venture using Mo Kα radiation (λ = 0.71073 Å) at 100 K and data were integrated using Apex III software. Crystal structures were solved using SHELXT and WinGX. All non-hydrogen atoms were refined anisotropically and all hydrogen atoms were treated isotropically. Images of the crystal structures and crystal packing were produced using Mercury 4.3.1. Hirshfeld surface analysis were carried out using Crystal Explorer 17.5 and the percentage contribution of short contacts were determined from 2D finger print plots.[67, 68]

UV-visible spectral studies were carried out using a Cary 5000 UV-Vis-NIR spectrophotometer (Varian Inc.). Fluorescence spectra were collected using Fluoromax-4 spectrofluorometer (Horiba Jobin Yvon. Cyclic voltammetry (CV) experiments were performed using Autolab P302N potentiostat/galvanostat with Nova 2.0 software. The electrochemical cell is consist with a glassy carbon disk electrode (3 mm diameter) as working electrode, Pt wire as counter electrode, and Ag/AgCl electrode as a quasi-reference electrode. 1,2-Difluorobenzene (DFB) (dried over flame-dried 4A MS) with 0.1 M tetrabutylammonium hexafluorophosphate ($TBAPF_6$) was used as electrolyte solution for the electrochemical experiments. All CV experiments were carried out inside an argon-filled glove box with O_2 and H_2O levels being controlled less than 0.1 ppm. Fc/Fc^+ redox couple was used to correct the final reported redox potential. All computational calculations were performed using the Gaussian 16; and GaussView 6.0 was used for processing the computational chemistry results.[69, 70]

Detailed synthetic procedures and characterization data of compounds 1 and 3, as well as detailed computational chemistry procedures were provided in Electronic Supplementary Information (**ESI**).

Crystallographic data:

Table 2: Summary of crystal data, data collection, and structure refinement parameters for 10, 13-dibromo-dibenzo [a,c]phenazine (**PBrDBP**), Compound **1** and Compound **3** with CCDC deposition numbers 2053442-2053444 respectively. Crystal structure of **PBrDBP** is provided in the supporting information. Compound **2** structure was published with a CCDC deposition number 968257.

	PBrDBP	Compound **1**	Compound **3**
CCDC#	2053442	2053443	2053444
Formula	C20 H10 Br2 N2	C26 H10 F14 N2	C26 H10 F14 N2
Formula wt	438.12	616.36	616.36
Temp, K	100	100	100
Crystal setting	Orthorhombic	Monoclinic	Monoclinic
Space group	P 21 21 21	P 21/c	C2/c
Hall symbol	-P 2ac 2ab	-P 2ybc	-C 2yc
International tables#	19	14	15
a, Å	4.2682	16.0011	23.9534
b, Å	18.1897	5.2318	13.3698
c, Å	19.6942	27.377	7.2037
α, deg	90	90	90
β, deg	90	101.533	93.922
γ, deg	90	90	90
z	4	4	4
Cell volume(Å^3)	1529.00	2245.6	2301.6
Density, g cm^{-3}	1.903	1.823	1.779
Ab coefficient, mm^{-1}	5.304	0.190	0.185
F (000)	856.0	1224	1224
Data range (θ_{min}-θ_{max})	2.35-31.32	2.19-25.98	2.98-34.33
Index ranges	±7,±31,±33	±19,±6,±33	±37,±21,±11
Measured reflections	26358	38876	30658
Independent reflections	8214	4440	4856
Reflections with I>2σ(I)	5153	3383	3129
Max/Min trans	0.400/0.620	0.982/0.989	0.985/0.974
Restraints/ Parameters	0/217	0/379	0/190
GOF	0.924	1.135	1.020
R [F^2>2 σ(F^2)]	0.0407	0.0483	0.0533
wR(F^2)	0.0847	0.1221	0.1581

Author contributions

H.S. and A.P. conceptualized and outlined the manuscript. A.P. synthesized and characterized compound **1**, collected single crystal XRD data, solved crystal structures, and performed computational study. S.G. synthesized and characterized compound **3**, and measured photophysical properties. Y.F. measured and analysed electrochemistry results. A.P. wrote the original draft of the manuscript and revised it with input from all authors. H.S. and A.P. finalized the manuscript. H.S. provided funding support through both federal and state grant agencies as listed in the acknowledgement section.

Conflicts of interest

Authors declare no competing financial interests.

Acknowledgements

Authors like to thank the U.S. Army Research Office (W911NF-09-10472) and the NSF (CHE1355677) for funding supports. Financial support from the South Dakota Governor's Office of Economic Development through the Center for Fluorinated Functional Materials are also appreciated. Bruker Dual Source Single-Crystal X-ray Diffractometer purchase was possible by funding from an NSF-MRI grant CHE-1919637. The authors like to thank the University of South Dakota Lawrence High-Performance Computing facility and the NSF (grant number: ACI-1626516) for providing computational resources. The authors thank Dr. Eduardo Callegari for assistance in acquiring mass spectra for compound **3**.

Notes and references

1. X. Zhang, H. Dong and W. Hu, *Adv. Mater.*, 2018, **30**, 1801048.
2. P. Yu, Y. Zhen, H. Dong and W. Hu, *Chem*, 2019, **5**, 2814-2853.
3. Q. Li and Z. Li, *Acc. Chem. Res.*, 2020, **53**, 962-973.
4. C. Sutton, C. Risko and J.-L. Brédas, *Chem. Mater.*, 2016, **28**, 3-16.
5. S. Tsuzuki, K. Honda, T. Uchimaru, M. Mikami and K. Tanabe, *J. Am. Chem. Soc.*, 2002, **124**, 104-112.
6. S. Tsuzuki, K. Honda, T. Uchimaru, M. Mikami and K. Tanabe, *J. Am. Chem. Soc.*, 2000, **122**, 3746-3753.
7. M. M. Payne, S. R. Parkin and J. E. Anthony, *J. Am. Chem. Soc.*, 2005, **127**, 8028-8029.
8. J. E. Anthony, *Chem. Rev.*, 2006, **106**, 5028-5048.
9. S. A. Sharber, R. N. Baral, F. Frausto, T. E. Haas, P. Müller and S. W. Thomas Iii, *J. Am. Chem. Soc.*, 2017, **139**, 5164-5174.
10. P. S. Salini, S. K. Rajagopal and M. Hariharan, *Cryst. Growth Des.*, 2016, **16**, 5822-5830.
11. Monika, A. Verma, M. K. Tiwari, B. Show and S. Saha, *ACS Omega*, 2020, **5**, 448-459.
12. K. E. Maly, *Cryst. Growth Des.*, 2011, **11**, 5628-5633.
13. U. H. F. Bunz, *Acc. Chem. Res.*, 2015, **48**, 1676-1686.
14. T. Higashino, S. Arai, S. Inoue, S. Tsuzuki, Y. Shimoi, S. Horiuchi, T. Hasegawa and R. Azumi, *CrystEngComm*, 2020, **22**, 3618-3626.
15. T. Schmaltz, B. Gothe, A. Krause, S. Leitherer, H.-G. Steinrück, M. Thoss, T. Clark and M. Halik, *ACS Nano*, 2017, **11**, 8747-8757.
16. H. Chen, W. Zhang, M. Li, G. He and X. Guo, *Chem. Rev.*, 2020, **120**, 2879-2949.

17. A. de Bettencourt-Dias, S. Viswanathan and K. Ruddy, *Cryst. Growth Des.*, 2005, **5**, 1477-1483.
18. N. Demir, G. Yakali, M. Karaman, Y. Gokpek, S. Denizalti, H. Bilgili, B. Dindar, S. Demic and M. Can, *J. Phys. Chem. C*, 2019, **123**, 21998-22008.
19. J.-H. Dou, Y.-Q. Zheng, Z.-F. Yao, Z.-A. Yu, T. Lei, X. Shen, X.-Y. Luo, J. Sun, S.-D. Zhang, Y.-F. Ding, G. Han, Y. Yi, J.-Y. Wang and J. Pei, *J. Am. Chem. Soc.*, 2015, **137**, 15947-15956.
20. D. Tian, Z. Ma, L. Gu, C. Zhou, C. Li, Z. Wang and H. Wang, *Cryst. Growth Des.*, 2020, **20**, 4479-4490.
21. A. K. Hailey, A. J. Petty Ii, J. Washbourne, K. J. Thorley, S. R. Parkin, J. E. Anthony and Y.-L. Loo, *Adv. Mater.*, 2017, **29**, 1700048.
22. R. Bu, F. Jiao, G. Liu, J. Zhao and C. Zhang, *Cryst. Growth Des.*, 2021, **21**, 3-15.
23. Q. Yue, Y.-Y. Wang, X.-L. Hu, W.-X. Guo and E.-Q. Gao, *CrystEngComm*, 2019, **21**, 6719-6732.
24. Q. Zhang, D. Chen, X. He, S. Huang, J. Huang, X. Zhou, Z. Yang, J. Li, H. Li and F. Nie, *CrystEngComm*, 2014, **16**, 10485-10491.
25. Y. Shang, R.-K. Huang, S.-L. Chen, C.-T. He, Z.-H. Yu, Z.-M. Ye, W.-X. Zhang and X.-M. Chen, *Cryst. Growth Des.*, 2020, **20**, 1891-1897.
26. G. R. Desiraju, *Acc. Chem. Res.*, 2002, **35**, 565-573.
27. P. Gómez, S. Georgakopoulos, M. Más-Montoya, J. Cerdá, J. Pérez, E. Ortí, J. Aragó and D. Curiel, *ACS Appl. Mater. Infterfaces*, 2021, **13**, 8620-8630.
28. J. Luo, J.-W. Wang, J.-H. Zhang, S. Lai and D.-C. Zhong, *CrystEngComm*, 2018, **20**, 5884-5898.
29. A. Priimagi, G. Cavallo, P. Metrangolo and G. Resnati, *Acc. Chem. Res.*, 2013, **46**, 2686-2695.
30. Y. Sakamoto and T. Suzuki, *J. Org. Chem.*, 2017, **82**, 8111-8116.
31. K. Merz, M. V. Evers, F. Uhl, R. I. Zubatyuk and O. V. Shishkin, *Cryst. Growth Des.*, 2014, **14**, 3124-3130.
32. S. Tsuzuki, *Annual Reports Section "C" (Physical Chemistry)*, 2012, **108**, 69-95.
33. P. Panini and D. Chopra, *CrystEngComm*, 2012, **14**, 1972-1989.
34. M. K. Ravva, C. Risko and J.-L. Brédas, in *Non-Covalent Interactions in Quantum Chemistry and Physics*, eds. A. Otero de la Roza and G. A. DiLabio, Elsevier, 2017, DOI: https://doi.org/10.1016/B978-0-12-809835-6.00011-6, pp. 277-302.
35. M. K. Corpinot and D.-K. Bučar, *Cryst. Growth Des.*, 2019, **19**, 1426-1453.
36. S. J. Nam, S. J. Jeon, Y. W. Han and D. K. Moon, *J. Ind. Eng. Chem.*, 2018, **63**, 191-200.
37. H. Usta, A. Facchetti and T. J. Marks, *Acc. Chem. Res.*, 2011, **44**, 501-510.
38. D. M. Cho, S. R. Parkin and M. D. Watson, *Org. Lett.*, 2005, **7**, 1067-1068.
39. K. P. Castro, T. T. Clikeman, N. J. DeWeerd, E. V. Bukovsky, K. C. Rippy, I. V. Kuvychko, G.-L. Hou, Y.-S. Chen, X.-B. Wang, S. H. Strauss and O. V. Boltalina, *Chem. Eur. J.*, 2016, **22**, 3930-3936.
40. L. Pilia, Y. Shuku, S. Dalgleish, D. W. M. Hofmann, N. Melis, K. Awaga and N. Robertson, *J. Organomet. Chem.*, 2020, **918**, 121277.
41. R. Schmidt, J. H. Oh, Y.-S. Sun, M. Deppisch, A.-M. Krause, K. Radacki, H. Braunschweig, M. Könemann, P. Erk, Z. Bao and F. Würthner, *J. Am. Chem. Soc.*, 2009, **131**, 6215-6228.
42. Y. Li, L. Tan, Z. Wang, H. Qian, Y. Shi and W. Hu, *Org. Lett.*, 2008, **10**, 529-532.
43. R. K. Radha Krishnan, B. J. Reeves, S. H. Strauss, O. V. Boltalina and B. Lüssem, *Org. Electron.*, 2020, **86**, 105898.
44. S. Yamada, K. Kinoshita, S. Iwama, T. Yamazaki, T. Kubota, T. Yajima, K. Yamamoto and S. Tahara, *Org. Biomol. Chem.*, 2017, **15**, 2522-2535.
45. W. Cao and E. M. Sletten, *J. Am. Chem. Soc.*, 2018, **140**, 2727-2730.
46. H. Sun, A. Putta, J. P. Kloster and U. K. Tottempudi, *Chem. Commun.*, 2012, **48**, 12085-12087.
47. Z. Zhang, J. Xiong, G. He, D. Dang, Y. Xie and Q. Wang, *Polym. Chem.*, 2020, **11**, 1307-1313.
48. I. Shulov, S. Oncul, A. Reisch, Y. Arntz, M. Collot, Y. Mely and A. S. Klymchenko, *Nanoscale*, 2015, **7**, 18198-18210.
49. B. A. Jones, A. Facchetti, M. R. Wasielewski and T. J. Marks, *J. Am. Chem. Soc.*, 2007, **129**, 15259-15278.
50. H. Sun, A. Putta and M. Billion, *J. Phys. Chem. A*, 2012, **116**, 8015-8022.
51. A. Putta, J. D. Mottishaw, Z. Wang and H. Sun, *Cryst. Growth Des.*, 2014, **14**, 350-356.
52. H. Sun, U. K. Tottempudi, J. D. Mottishaw, P. N. Basa, A. Putta and A. G. Sykes, *Cryst. Growth Des.*, 2012, **12**, 5655-5662.
53. M. O. BaniKhaled, J. D. Mottishaw and H. Sun, *Cryst. Growth Des.*, 2015, **15**, 2235-2242.
54. Z.-H. Guo, T. Lei, Z.-X. Jin, J.-Y. Wang and J. Pei, *Org. Lett.*, 2013, **15**, 3530-3533.
55. Y. Liu, Y. Chen, H. Li, S. Wang, X. Wu, H. Tong and L. Wang, *ACS Appl. Mater. Infterfaces*, 2020, **12**, 30652-30658.
56. J. Shi, J. Chen, Z. Chai, H. Wang, R. Tang, K. Fan, M. Wu, H. Han, J. Qin, T. Peng, Q. Li and Z. Li, *J. Mater. Chem.*, 2012, **22**, 18830-18838.
57. H. Deol, G. Singh, M. Kumar and V. Bhalla, *J. Org. Chem.*, 2020, **85**, 11080-11093.
58. M. Li, C. An, T. Marszalek, X. Guo, Y.-Z. Long, H. Yin, C. Gu, M. Baumgarten, W. Pisula and K. Müllen, *Chem. Mater.*, 2015, **27**, 2218-2223.
59. P. K. Sahoo, C. Giri, T. S. Haldar, R. Puttreddy, K. Rissanen and P. Mal, *Eur. J. Org. Chem.*, 2016, **2016**, 1283-1291.
60. Y. Yang, A. Li, Z. Ma, J. Liu, W. Xu, Z. Ma and X. Jia, *Dyes Pigm.*, 2020, **181**, 108575.
61. M. O. BaniKhaled, J. D. Becker, M. Koppang and H. Sun, *Cryst. Growth Des.*, 2016, **16**, 1869-1878.
62. C. Hansch, A. Leo and R. W. Taft, *Chem. Rev.*, 1991, **91**, 165-195.
63. M. W. Day, X. A. Amashukeli and H. B. Gray, *CSD Communication*, 2002, DOI: 10.5517/cc4rt0p.
64. Y. Zhao and D. G. Truhlar, *Theor. Chem. Acc.*, 2008, **120**, 215-241.
65. A. Schäfer, C. Huber and R. Ahlrichs, *J. Chem. Phys.*, 1994, **100**, 5829-5835.
66. J. B. Foresman and A. E. Frisch, *Exploring Chemistry with Electronic Structure Methods*, Gaussian, Inc. Wallingford, CT. 2015.
67. M. A. Spackman and D. Jayatilaka, *CrystEngComm*, 2009, **11**, 19-32.
68. M. A. Spackman and J. J. McKinnon, *CrystEngComm*, 2002, **4**, 378-392.

69. M. J. Frisch, G. W. Trucks, H. B. Schlegel, G. E. Scuseria, M. A. Robb, J. R. Cheeseman, G. Scalmani, V. Barone, G. A. Petersson, H. Nakatsuji, X. Li, M. Caricato, A. V. Marenich, J. Bloino, B. G. Janesko, R. Gomperts, B. Mennucci, H. P. Hratchian, J. V. Ortiz, A. F. Izmaylov, J. L. Sonnenberg, Williams, F. Ding, F. Lipparini, F. Egidi, J. Goings, B. Peng, A. Petrone, T. Henderson, D. Ranasinghe, V. G. Zakrzewski, J. Gao, N. Rega, G. Zheng, W. Liang, M. Hada, M. Ehara, K. Toyota, R. Fukuda, J. Hasegawa, M. Ishida, T. Nakajima, Y. Honda, O. Kitao, H. Nakai, T. Vreven, K. Throssell, J. A. Montgomery Jr., J. E. Peralta, F. Ogliaro, M. J. Bearpark, J. J. Heyd, E. N. Brothers, K. N. Kudin, V. N. Staroverov, T. A. Keith, R. Kobayashi, J. Normand, K. Raghavachari, A. P. Rendell, J. C. Burant, S. S. Iyengar, J. Tomasi, M. Cossi, J. M. Millam, M. Klene, C. Adamo, R. Cammi, J. W. Ochterski, R. L. Martin, K. Morokuma, O. Farkas, J. B. Foresman and D. J. Fox, *Gaussian 16, Rev. C.01*, Gaussian, Inc., Wallingford CT, 2016.
70. R. Dennington, T. A. Keith and J. M. Millam, *Semichem Inc.*, Shawnee Mission, KS, 2016.

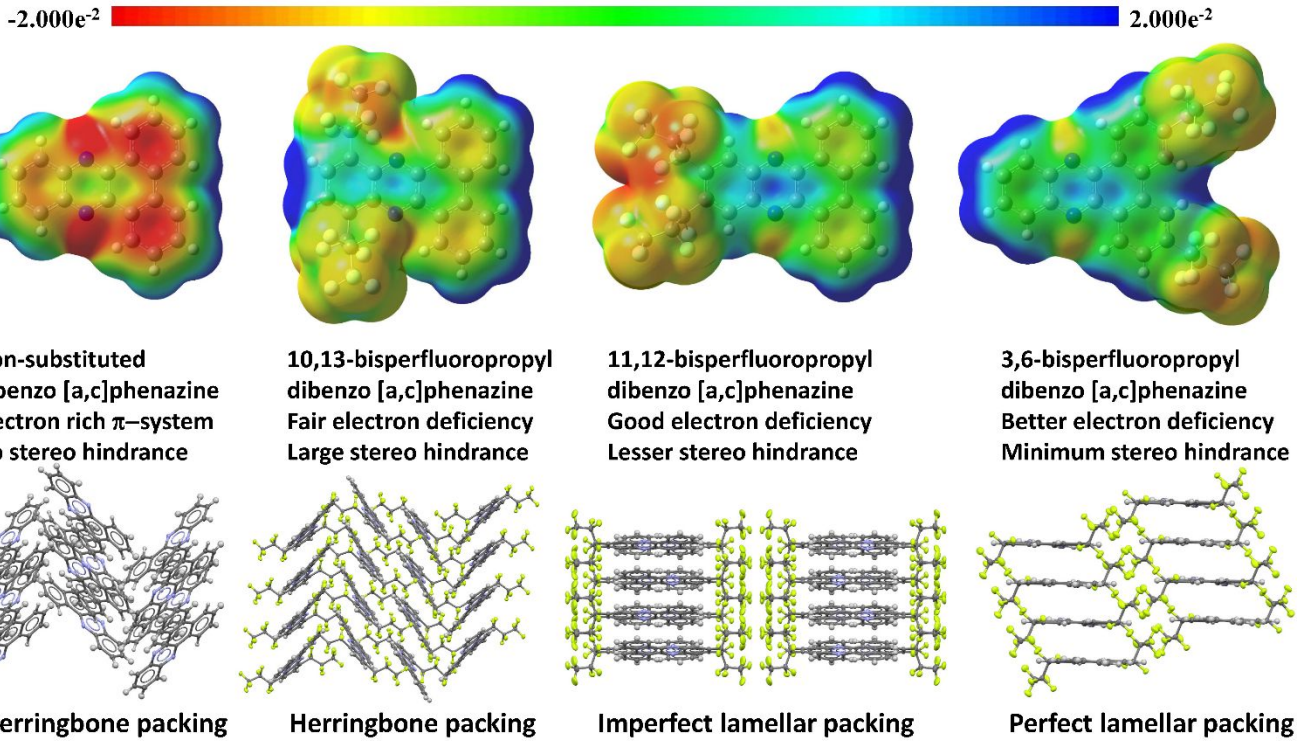
-2.000e-2
2.000e-2
Non-substituted
dibenzo [a,c]phenazine
Electron rich π–system
No stereo hindrance
10,13-bisperfluoropropyl
dibenzo [a,c]phenazine
Fair electron deficiency
Large stereo hindrance
11,12-bisperfluoropropyl
dibenzo [a,c]phenazine
Good electron deficiency
Lesser stereo hindrance
3,6-bisperfluoropropyl
dibenzo [a,c]phenazine
Better electron deficiency
Minimum stereo hindrance
Herringbone packing
Herringbone packing
Imperfect lamellar packing
Perfect lamellar packing